Multinuclear Solid-State NMR Characterization, Ion Dissociation, and Dynamic Properties of Lithium-Doped Organic−Inorganic Hybrid Electrolytes Based on Ureasils

Hsien-Ming Kao,*,† Tzu-Ti Hung,† and George T. K. Fey‡

Departments of Chemistry and Chemical and Materials Engineering, National Central University, Chung-Li, Taiwan 32054, R.O.C.

Received July 12, 2007; Revised Manuscript Received September 17, 2007

ABSTRACT: Solid organic−inorganic hybrid electrolytes based on diureasils doped with $LiClO_4$ have been obtained by the sol−gel process through the reaction of poly(propylene glycol)-*block*-poly(ethylene glycol)-*block*-poly(propylene glycol) bis(2-aminopropyl ether) ($H_2N-PPG-PEG-PPG-NH_2$) with 3-isocyanatepropyltriethoxysilane (ICPTES), followed by co-condensation of an epoxy trialkoxysilane, 3-(glycidyloxypropyl)-trimethoxylsilane (GLYMO). The structural and dynamic properties of the materials were systematically investigated by a variety of techniques including ac impedance, Fourier transform infrared spectroscopy (FTIR), differential scanning calorimetry (DSC), multinuclear (^{13}C, ^{29}Si, ^{7}Li) solid-state NMR, $^{1}H-^{13}C$ 2D WISE (wide-line separation) NMR, and ^{7}Li pulsed gradient spin−echo (PGSE) NMR measurements. The length of backbone PEG chain, the extent of GLYMO cross-linking, and the salt concentration were varied in order to obtain the materials with high conductivities. A maximum ionic conductivity value of 1.37×10^{-5} S/cm was obtained at 30 °C for the hybrid electrolyte with a [O]/[Li] ratio of 32. This ionic conductivity value is 1 order of magnitude higher than that of previously characterized electrolytes based on ureasils without incorporation of GLYMO. The results of ^{13}C cross-polarization magic-angle spinning (CPMAS) NMR with varying contact times and $^{1}H-^{13}C$ WISE NMR provided a microscopic view of the effects of salt concentrations on the dynamic behavior of the polymer chains. Only one distinct ^{7}Li local environment was detected by variable temperature $^{7}Li-\{^{1}H\}$ MAS NMR. The temperature dependence of ^{7}Li static line widths and self-diffusion coefficients showed that there is a strong correlation between the dynamic properties of the charge carriers and the bulk ionic conductivity.

Introduction

Solid polymer electrolytes (SPEs) formed by complexing alkali metal salts (LiX) with an ion-conducting polymer have received considerable attention because of their potential applications in solid-state batteries, chemical sensors, data storage, and electrochemical devices.[1−5] These polymer electrolytes have to satisfy several requirements, including high ionic conductivity, good mechanical properties, and excellent electrochemical stability. Although lithium doped polyethylene oxide (PEO) based SPE systems were first recognized with ionic conductivity, it was soon realized that their performance was often hindered by crystallization of PEO, leading to its low conductivity at ambient temperature. Furthermore, for many battery applications, even high molecular weight PEO based electrolytes have unacceptable mechanical properties and low processability, especially at higher temperatures. The ionic conductivity of SPEs is due to the motion of dissolved ionic species (cations and anions) in a polymeric matrix. It is recognized that ion conduction occurs exclusively in the amorphous phase in pure polymer electrolytes,[6] above the glass transition temperature (T_g), via a liquidlike motion of the cations assisted by the segmental reorientations of the neighboring polymer chains, although some recent studies showed that the ion transport associated with the crystalline phase can also yield a significant contribution to the conductivity under appropriate circumstances.[7−10] Thus, increasing the volume fraction of the amorphous domain in the polymer host and decreasing its T_g appear to be the main strategy to obtain better conductivity for SPEs. A variety of amorphous materials with low T_g have been developed.[11−14] Recent work has utilized various approaches to suppress the crystallinity through the incorporation of oxymethylene groups to PEO.[11,12] In addition, low T_g polyphosphazenes[13,14] and polysiloxanes[11,12] with oligoether side groups attached to the flexible backbones have been used effectively.

In search for better polymer host matrices, much effort has been devoted to develop new polymer electrolyte systems such as copolymers[15] and blends[16] or materials doped with nanosized fillers, classified as composite electrolytes.[17] Positive effects of the incorporation of the inorganic filler have been observed for fully amorphous polymers.[18] A more favorable strategy is to develop organic−inorganic hybrid electrolytes, so-called ormolytes (organically modified electrolytes) via in situ formation of inorganic component within the polymer matrix. The organic−inorganic hybrid electrolytes are often prepared via a simple sol−gel synthetic route, through the use of functionalized organosilanes to combine with the polymer backbones, without recourse to complex synthesis procedures.[19−31] These materials take advantage of the rich chemistry of silicon-based structure networks to provide a relatively stable three-dimensional matrix, which can be readily tailored to obtain the desired chemical and physical properties. With dependence on the reaction conditions and the ratio of organic and inorganic components, organic and inorganic components can be either merely intimately mixed or chemically bonded. Two types of hybrids have been classified according to the interactions between organic−inorganic interfaces: type I hybrids, in which weak interactions such as van der Waals contacts, hydrogen bonding, or electro-

* Corresponding author. Hsien-Ming Kao, fax: +886-4227664. Phone: +886-4275054. E-mail: hmkao@cc.ncu.edu.tw.
† Department of Chemistry.
‡ Department of Chemical and Materials Engineering.

10.1021/ma071541c CCC: $37.00
Published on Web 11/01/2007

static interactions are established between both components (one acts as host network and the other as entrapped species),[23,34−37] and type II hybrids, in which at least a proportion of the organic and inorganic components are bonded by means of strong chemical interactions such as covalent bonds.[38,39] The type I hybrids, in general, have higher room-temperature ionic conductivities (up to 10^{-4} S/cm) than the type II hybrids but unfortunately with much lower chemical stability. The structural and electrical properties of these two types of hybrids are strongly dependent on the synthesis conditions such as the polymer molecular weights, the lithium concentration, the weight percent of polymer, and the interactions between the organic−inorganic phases.[19] In most of cases, the incorporation of a silicate network into the polymer matrix permits not only a significant reduction or even suppression of crystallinity but may also result in a marked improvement in the mechanical resistance and the chemical/thermal stability of the materials. Therefore, the hybrid polymer electrolytes with controlled chemical and physical properties are promising candidates to overcome the disadvantages associated with conventional PEO-based electrolytes.

Among the various organic−inorganic hybrids that have been proposed in the literature, a family of versatile compounds is noteworthy, classified as diureasils, in which polyether-based chains of variable lengths are grafted on both ends to silicate backbones through urea functionalities.[20,40−42] Therefore, the matrix of the so-called ureasils belongs to the family of type II hybrids. Generally, the oxyethylene segments of a commercial polymer containing diamine groups were bonded to a silica matrix through urea (−NH(C═O)NH−) bridges to yield a semicrystalline macromolecular structure with high optical transparency, good thermal stability, and encouraging chemical and mechanical properties. The ureasil structures have been investigated very recently by IR[43] and photoluminescence spectroscopies.[44] The chemical and electrochemical properties of the ureasil-based electrolytes synthesized through the addition of controlled quantities of various salts such as $LiClO_4$ or $LiCF_3SO_3$ to a diureasil hybrid host matrix for the potential use in lithium ion batteries have also been reported.[25,45,46] The urea linkage in these electrolytes provides anchoring points for the chains, making these polymer electrolytes fully amorphous. The amorphous nature of the ureasils allows these materials to be promising candidates for use as ion-conducting polymer electrolytes with no detrimental effects by crystallization. When doped with lithium salts, however, the ionic conductivity of these electrolytes is relatively low at room temperature (only up to 10^{-6} S/cm). The effects of the synthesis conditions on the dynamic properties of diureasil based hybrids are still not fully investigated. The information about their microscopic molecular behavior should be considered to be a key point for the optimization of the properties of these hybrids. For this purpose, solid-state NMR spectroscopy can make important contributions.

In the present work, organic−inorganic hybrid electrolytes based on the host diureasils have been prepared by reacting $H_2N-PPG-PEG-PPG-NH_2$ triblock copolymer, where PPG and PEG represent poly(propylene glycol) and poly(ethylene glycol), respectively, with 3-isocyanatepropyltriethoxysilane (ICPTES) to form a diureasil hybrid precursor, followed by the co-condensation with (3-glycidyloxypropyl)trimethoxysilane (GLYMO) as another silica source to yield materials with totally amorphous nature and good conductivity. As shown in Scheme 1, hydrolysis of GLYMO, followed by condensation and polymerization with the preformed diureasil precursor, leads to fresh inorganic components that are intimately mixed with the

Scheme 1. Schematic Representation of the Synthesis and Structure of the Present Hybrid Electrolyte

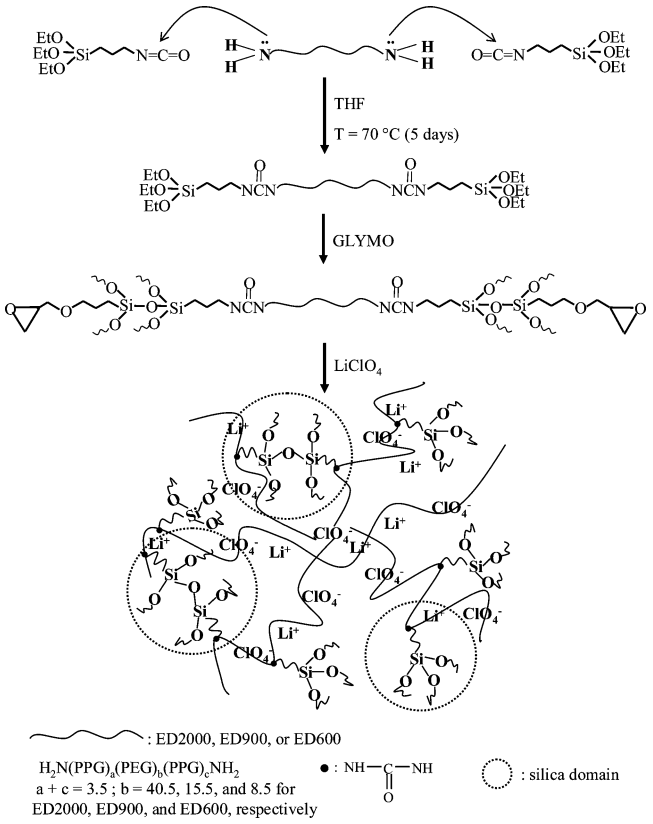

polymer host. It is important to emphasize that the multicomponent nature of this system allows the physical and chemical properties of these SPEs to be tunable through optimization of the polymer segment length, the salt concentration, and the silica content. Moreover, the functionality, i.e., the N═C═O group, in ICPTES provides a cross-linking center to interact with the amine end groups of the triblock copolymer to generate a semicrystalline diureasil precursor. Then the diureasil precursor further condenses with GLYMO and results in reinforcement of the rubbery network and thereby improves the mechanical properties of the hybrid materials. This paper highlights the use of multinuclear (^{13}C, ^{29}Si, ^{7}Li) solid-state NMR techniques in combination with the measurements of Li^+ diffusion coefficients, a parameter directly related to ionic conductivity, using pulsed gradient spin−echo (PGSE) NMR techniques, in order to gain more insights into the role for ion−polymer interactions, the nature of the charge carrier, and the ionic association process in the ionic conductivity. These NMR results were combined with the infrared (IR), differential scanning calorimetry (DSC), and ionic conductivity results for further discussion and elucidation of the influence of the material composition on their properties.

Experimental Section

Preparation of Hybrid Electrolyte Films. Lithium perchlorate ($LiClO_4$, Alfa Aesar) and $H_2N-PPG-PEG-PPG-NH_2$ triblock copolymer (Aldrich, commercially designated by Jeffamine ED2000, ED900, and ED600 with M_w = 2000, 900, and 600 g/mol containing about 40.5, 15.5, and 8.5 PEG units, respectively) were dried under vacuum for several days prior to use. Since the relative ratios between the ethylene oxide and the propylene oxide units in the polymer play a key role in ion transport, a series of polymers with fixed PPG segments but varying PEG segments were used. 3-Isocyanatepropyltriethoxysilane (ICPTES, Aldrich) and 3-(glycidyloxypropyl)trimethoxysilane (GLYMO, Aldrich) were used as

received. Tetrahydrofuran (THF) was distilled from sodium/benzophenone prior to use. The previously reported procedures for the synthesis of Li^+-based diureasils were slightly modified in this study. The preliminary step of the preparation of the diureasils involves the formation of urea linkages between the terminal amine groups of a doubly functional oligopolyoxyethylene segment and the isocyanate group of ICPTES with a molar ratio of 1:2 in an anhydrous THF solution (10 mL). The resulting solution was stirred at 70 °C for 5 days to yield a stable diurea cross-linked hybrid precursor molecule, as illustrated in Scheme 1. This process was adopted for polymers with different molecular weights. The grafting process was monitored by infrared spectroscopy. The intensity of the isocyanate vibrational band at approximately 2273 cm^{-1} was progressively decreased as the reaction proceeded, finally disappearing when the reaction was complete. These spectral changes were accompanied by the growth of a series of bands due to the presence of urea groups in the region between 1800 and 1500 cm^{-1}.

GLYMO was incorporated in the second step of the synthesis procedure. The inorganic part of the hybrid was further prepared by mixing 2.5 g of the diureasil precursor in 30 mL of acetonitrile with the desired amount of GLYMO in the presence of 2 mL of 2 M HCl at room temperature, and the resulting mixture was stirred for 1 h. Afterward, appropriate amounts of $LiClO_4$ were added into the solution to achieve the desired [O]/[Li] ratios. The solutions were then stirred at room temperature for another hour. The casting solution was put into Telfon dishes, and the solvent was slowly evaporated at room temperature for 24 h. The materials were then heated gradually from 30 to 80 °C under vacuum for several days to give a piece of transparent and crack-free film with good mechanical strength and a good degree of elasticity. The resulting hybrid electrolytes were designated as G(*X*)-U(*Y*)-*Z*, where G stands for GLYMO, *X* the molar ratio of GLYMO/polymer, U(*Y*) represents the host diureasil framework (U denotes the urea group, and the number *Y* corresponds to the average molecular weight of the starting polymer, either 2000, 900, or 600), and *Z* (salt composition) indicates the number of ether oxygen atoms (only for polymer) per Li^+ cation. The films were then stored in a glovebox under a nitrogen atmosphere for further measurements. The thickness of the films was controlled to be in the range of 150−200 μm. The cross-linked polymer films are strong and highly elastic in nature.

DSC Thermograms. Differential scanning calorimetry (DSC) was performed in the temperature range from −60 to 125 °C using a Perkin-Elmer DSC 7 calorimeter at a heating rate of 5 °C/min. The sample weights were maintained in the range of 5−20 mg and were hermetically sealed in aluminum pans. Glass transition temperatures (T_g) were then determined using the fictive temperature method in the Pyris software. The reported DSC curves are the second heating scans taken after an initial heating scan to erase the thermal history, followed by quenching to −100 °C.

FTIR Spectroscopy. FTIR spectra were obtained from a Bio-Rad FTS155 spectrometer at a resolution of 4 cm^{-1} using the KBr wafer technique. Band deconvolution of the resulting spectra was conducted to obtain the best fit for the band envelope.

ac Impedance Measurements. Alternating current (ac) impedance measurements of the hybrid electrolytes were performed using a frequency response analyzer Autolab/PGSTAT 30 electrochemical instrument over a frequency range of 10 Hz−1 MHz with an amplitude of 10 mV. All the specimens were sandwiched by two polished stainless steel blocking electrodes for conductivity tests. These measurements were performed at the temperature in the range of 10−75 °C. Each sample was thermally equilibrated at each selected temperature for at least 1 h prior to taking measurements. Impedance plots of the complexes (semicircles) were computed from the raw experimental data. The intersection in the imaginary impedance at low frequency with the real impedance axis corresponds to the ionic conductance of the samples, and hence the conductivity values (σ) are obtained from the equation $\sigma = (1/R_b)(t/A)$, where R_b is the bulk resistance, t is the thickness, and A is the area of the sample.

Solid-State NMR Measurements. Solid-state NMR experiments were performed on a Varian Infinityplus-500 NMR spectrometer, equipped with a Chemagnetics 7.5 mm MAS probe and a double-tuned static probe. The Larmor frequencies for ^{7}Li, ^{13}C, and ^{29}Si nuclei are, respectively, 194.3, 125.7, and 99.3 MHz. Magic angle spinning conditions in the range of 3−5 kHz were employed to record ^{13}C and ^{29}Si NMR spectra and some ^{7}Li NMR spectra. The $\pi/2$ pulse lengths for ^{7}Li and ^{29}Si nuclei were typically 4 and 6 μs, respectively. The ^{13}C and ^{29}Si chemical shifts were externally referenced to tetramethylsilane (TMS) at 0 ppm. The ^{1}H → ^{13}C cross-polarization magic-angle spinning(CPMAS) NMR spectra were also recorded as a function of CP contact time ranging from 0.2 to 18 ms. ^{7}Li NMR spectra were acquired under either static or MAS conditions with and without proton decoupling during the acquisition. The static ^{7}Li line widths were taken to be the full-width at half-height (FWHH) of the peaks and measured as a function of temperature from −100 to 80 °C. Variable temperature ^{7}Li−{^{1}H} (i.e., proton decoupled) MAS NMR spectra were acquired to reveal different local environments of the lithium cations. ^{7}Li chemical shifts were externally referenced to an 1 M LiCl(aq) at 0 ppm.

2D ^{1}H−^{13}C WISE Experiments. ^{1}H wide-line spectra were acquired with the use of the 2D WISE (wideline separation spectroscopy) NMR pulse sequence developed by Schmidt-Rohr et al.[47] The pulse sequence consists of a 90_x degree pulse on the protons, which flips the magnetization into the *xy* plane, followed by a t_1 evolution period. The proton magnetization evolves under the influence of dipolar coupling during the time t_1. Then a 90_{-x} degree pulse is applied to flip the magnetization back to the *z*-axis. In the simplest version of this experiment with the mixing time $t_m = 0$, the proton magnetization is transferred to the carbons by means of CP processes and the corresponding ^{13}C signal is detected under conditions of MAS and proton decoupling during the acquisition time t_2. For each of these resolved ^{13}C signals, a corresponding ^{1}H line can be obtained in this way. Therefore, a correlation can be made between the chemical structure and segmental mobility of the polymer. Spectral widths of 40 and 100 kHz were used for the ω_2 and ω_1 dimensions, respectively. Typically 128 t_1 increments were used in the 2D WISE experiments. The CP and the dipolar decoupling field strengths were the same as those used for the ^{13}C CPMAS NMR experiments.

Pulsed Gradient Spin−Echo NMR. PGSE NMR experiments were employed in this study to measure the ^{7}Li diffusion coefficients. The PGSE NMR experiments were performed using a Doty 5 mm dual broad band gradient probe and a current amplifier provided by Varian. The PGSE pulse sequence consists of a 90° pulse followed by two identical gradient pulses, separated by a 180° pulse, which attenuate the echo intensity while the observed nuclei are diffusing. The echo attenuation is directly related to the diffusion coefficient, D, of the observed ^{7}Li spins, and the experimental parameters of the PGSE pulse sequence according to the Stejskal−Tanner equation:[48]

$$I = I_0 \exp[-\gamma^2\delta^2 g^2(\Delta - \delta/3)D] \quad (1)$$

where I and I_0 are the echo amplitudes obtained with and without application of the gradient pulses, respectively, γ the gyromagnetic ratio of the observed ^{7}Li nuclei, δ the width of the gradient pulse, g the magnetic field gradient amplitude, and Δ the time interval between the leading edges of the gradient pulses. For each PGSE experiment, the gradient strength was varied while keeping all other parameters constant. The gradient strength was calibrated by measuring the known self-diffusion coefficient of H_2O at 25 °C (2.23×10^{-5} cm^2/s).[49] The ^{7}Li diffusion coefficients can be obtained from the slope of the plots of $\ln(I/I_0)$ against $\gamma^2\delta^2 g^2(\Delta - \delta/3)$. Measurements were carried out on about 500 mg samples which were loaded and packed into 5 mm Pyrex tubes in a very low humidity (<1 ppm) glovebox. The Pyrex tubes were then flame sealed under vacuum. The self-diffusion coefficients were obtained in the temperature range of 40−120 °C. The typical reproducibility of the diffusion coefficient measurements is about ±3%.

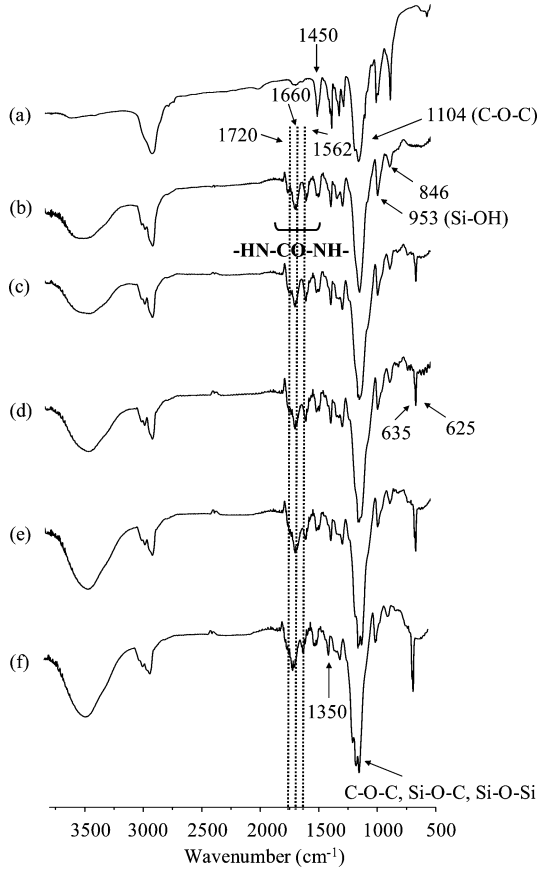

Figure 1. FTIR spectra of (a) ED2000, (b) G(0)-U(2000)-∞, and G(1)-U(2000)-*Z* hybrid electrolytes with various [O]/[Li] ratios, where *Z* = (c) 32, (d) 24, (e) 16, and (f) 8.

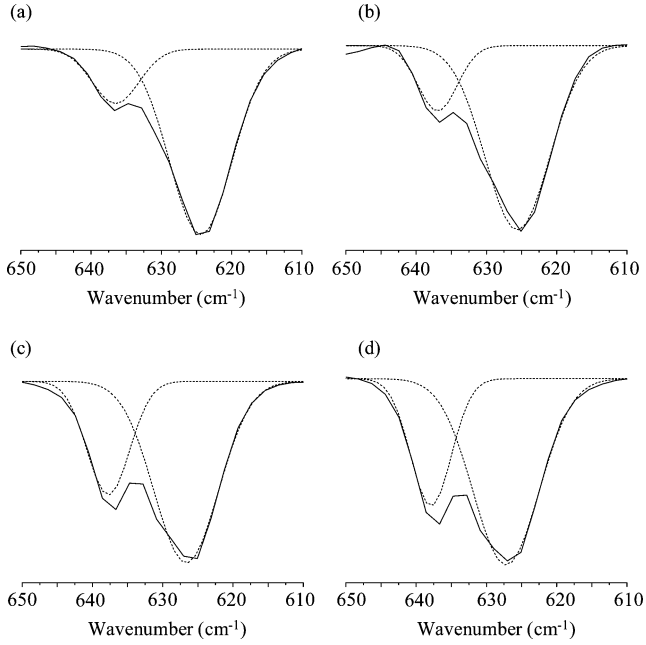

Figure 2. IR fitting results (in the range of 600−650 cm^{-1}) of G(1)-U(2000)-*Z* hybrid electrolytes with various [O]/[Li] ratios, where *Z* = (a) 32, (b) 24, (c) 16, and (d) 8.

Results and Discussion

Structure of Diureasil Based Electrolytes. IR. Infrared spectroscopy is a convenient method to trace the reaction of isocyanate for ureasil preparation and also can provide the information about the development of an organic−inorganic network. Figure 1 shows the FTIR spectra of the parent polymer ED2000, the ureasil precursor (without GLYMO and salt), and G(1)-U(2000)-*Z* hybrid electrolytes with various $LiClO_4$ concentrations. Previous spectroscopic studies carried out by Coleman et al. revealed that polyurethane exhibited bands at 3440 and 3320 cm^{-1} due to the free and hydrogen-bonded N−H stretching modes, respectively.[50] As seen in Figure 1, the high-frequency region of the IR spectra was ill-defined and exhibited only a broad band. Therefore, we focused on another spectral region where the main absorption bands produced by the vibrations of the urea groups occurred, so-called amide I and II vibrations. When ED2000 reacted with ICPTES to form the diureasil precursor, the formation of the urea groups gave new peaks appearing in the region between 1800 and 1500 cm^{-1}. These peaks did not have any significant changes after GLYMO incorporation and Li salt doping. The urea cross-links in ureasils contains active centers capable of participating in hydrogen bonds, which structurally resemble the polyurethane block polymers. Previous IR spectroscopic studies have confirmed that two hydrogen-bonded urea−polyether structures are present in the undoped ureasil material.[43] The amide I band involves the C═O stretching, the C−N stretching, and the C−C−N deformation vibrations,[51] which is highly sensitive to hydrogen bonding. A band at 1732 cm^{-1}, associated with carbonyls free of hydrogen bonding, and another one at 1703 cm^{-1}, attributed to hydrogen-bonded carbonyls, have been observed in the spectra of model polyurethanes.[52] We thus assigned the bands at 1720 and 1660 cm^{-1} (Figure 1) to the amide I modes without and with hydrogen bonding, respectively. The amide II band involves the vibration of the N−H in-plane bending, the C−N stretching, and the C−C stretching modes.[51,53] The medium intensity band observed at 1562 cm^{-1} is attributed to the amide II mode.[44] The presence of the characteristic bands associated with the urea linkage confirmed a successful synthesis of the ureasil hybrid.

A major peak associated with C−O−C stretching vibrations was observed at 1104 cm^{-1} for the parent ED2000. With the addition of the lithium salts, two sharp peaks at 1120 and 1110 cm^{-1} appeared, suggesting that the ether group of ED2000 had some interactions with the added lithium cations. Although changes in the intensity, shape, and position of the C−O−C stretching mode were associated with the polyether−$LiClO_4$ interactions, the dependence of the absorption peak of C−O−C stretching vibrations on the salt concentrations was not clarified in the IR spectra, since the characteristic absorption bands of the hydrolysis product (Si−O−C and Si−O−Si) of ICPTES and GLYMO were also expected to appear in the same region.[54,55]

Ion Dissociation. The ClO_4^- anion is an excellent probe that allows the extent of ionic association to be estimated. The characteristic $\nu(ClO_4^-)$ mode of $LiClO_4$ is particularly sensitive in changing the ion−ion interactions in the electrolyte systems. Two bands at 625 and 635 cm^{-1} due to the vibration modes of ClO_4^- ions were observed. According to previous literature,[56−58] the band centered at 625 cm^{-1} has been assigned to the vibration of the "free" ClO_4^- anion, which does not interact directly with lithium cations, and the band centered at 635 cm^{-1} to the vibration of the $Li^+ClO_4^-$ contact-ion pairs. To investigate the behavior of ion association in the present hybrid system, the spectral features of the $\nu(ClO_4^-)$ mode were fitted with Gaussian−Lorentzian functions, and the results are displayed in Figure 2 for G(1)-U(2000)-*Z* samples and in Figures S1 and S2 (Supporting Information) for G(1)-U(900)-*Z* and G(1)-U(600)-*Z* samples, respectively. The fractions of "free" cations as a function of salt concentration for the hybrid electrolytes

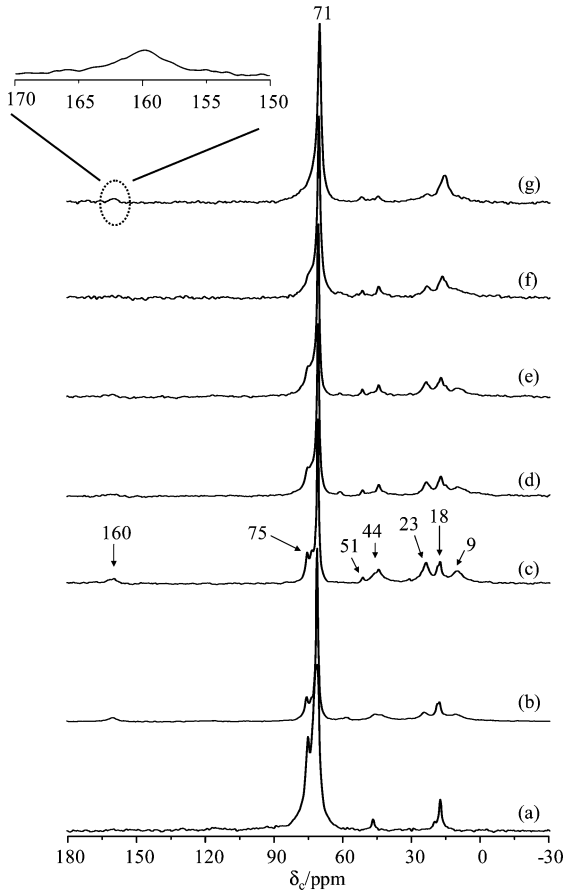

Figure 3. ^{13}C CPMAS NMR spectra of (a) ED2000, (b) G(0)-U(2000)-∞, and G(1)-U(2000)-*Z* hybrid electrolytes with various [O]/[Li] ratios, where *Z* = (c) ∞, (d) 32, (e) 24, (f) 16, and (g) 8.

Table 1. Conductivity (at 30 °C) and FTIR Deconvolution Results of the G(1)-U(*Y*)-Z Hybrid Electrolytes Studied

	G(1)-U(2000)		G(1)-U(900)		G(1)-U(600)	
Z, [O]/[Li]	σ (S/cm)	free ClO_4^-, %	σ (S/cm)	free ClO_4^-, %	σ (S/cm)	free ClO_4^-, %
32	1.37×10^{-5}	82	2.46×10^{-6}	79	2.75×10^{-7}	78
24	7.49×10^{-6}	81	2.16×10^{-6}	75	3.22×10^{-7}	75
16	6.45×10^{-6}	71	2.17×10^{-6}	71	7.38×10^{-8}	70
8	1.21×10^{-6}	70	9.78×10^{-7}	70	1.33×10^{-7}	69

are given in Table 1, which were calculated as the ratio of the area under the 625 cm^{-1} mode to the total area under the $\nu(ClO_4^-)$ envelope. About 80% of ClO_4^- exists as spectroscopically "free" species for G(1)-U(2000)-32 and G(1)-U(2000)-24, while about 70% of free ClO_4^- was observed for other electrolytes with higher salt concentrations (Table 1). This is as expected since more and more free ions become bound with the opposite ions to form contact ions upon addition of more salts. As a result, the content of the free ions decreased. The degree of ion dissociation slightly decreased or remained unchanged when the molecular weight of the polymer host changed from 2000 to 600 g/mol (Table 1), indicating that the fraction of the PEG segment did not make significant contribution to ion dissociation at a given [O]/[Li] ratio.

^{13}C CPMAS NMR. Figure 3 shows the ^{13}C CPMAS NMR spectra of the parent ED2000, the ureasil precursor (without GLYMO and salt), and G(1)-U(2000)-*Z* hybrid electrolytes with various salt contents. The most predominant peak at 71 ppm is assigned to methylene carbons adjacent to the ether oxygen of the polymer chain. The methyl carbon from the propylene oxide units appear at 18 ppm, while the peak at 47 ppm can be assigned to the nitrogen substituted carbons at the terminal of the diamines. Two peaks at 23 and 9 ppm were clearly visible when GLYMO was incorporated and are assigned to the methylene carbons in the α and *β* positions to the silicon atom of GLYMO, respectively, while the peaks at 44 and 51 ppm expected for the carbon atoms in the epoxide ring of GLYMO were also observed, indicative of the incompleteness of the epoxide ring opening. Besides the major peak at 71 ppm, there is a smaller peak at 75 ppm due to the ether carbons in the PPG segments, which is also clearly resolved for the parent ED2000. This peak became a broader shoulder and was no longer resolved when the salt doping level was high. The peak at 73 ppm can be assigned to the carbon attached to ether oxygens of GLYMO, while a small peak at around 60 ppm is due to the formation of diol function from the polymerization reaction of GLYMO.[59] The high level of salt doping causes a more broad distribution of the environments of the polymer chains, which results in a broader low-field shoulder near the peak at 71 ppm (Figure 3f,g). For example, the line width (FWHH) of the peak at 71 ppm progressively increased from 120 Hz for G(1)-U(2000)-∞ to 220 Hz for G(1)-U(2000)-8. The urea functional groups of this hybrid matrix, which are considerably less abundant, gave rise to a very weak signal at 160 ppm of the Li^+-doped hybrid electrolytes (see inset, Figure 3). This confirmed the formation of urea linkages between the polymer diamine and ICPTES.

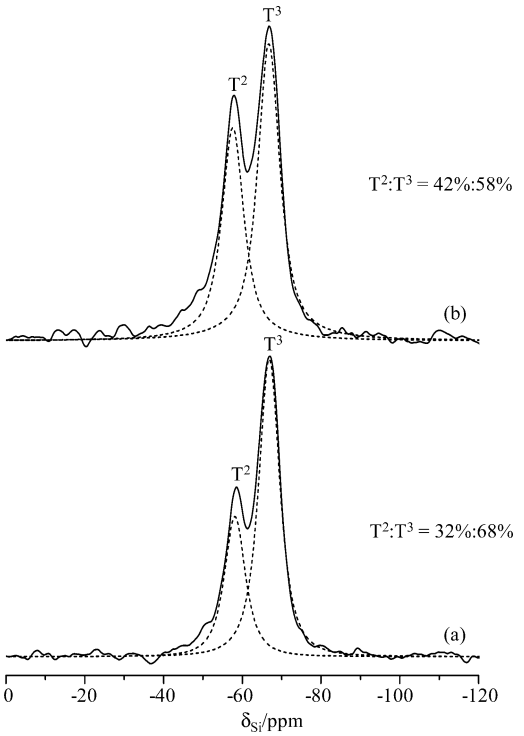

Figure 4. ^{29}Si MAS NMR spectra of (a) G(1)-U(2000)-32 and (b) G(1)-U(2000)-8 hybrid electrolytes. The dashed lines represent the components used for the spectral deconvolution.

^{29}Si MAS NMR. ^{29}Si MAS NMR is a direct method to characterize the silicon condensation and to indicate the silica network architecture inside these hybrid materials. As shown in Figure 4, two signals at −67 and −57 ppm, corresponding to T^3 ($RSi(OSi)_3$, R = alkyl group) and T^2 ($RSi(OSi)_2(OH)$) sites, were observed for the two selected G(1)-U(2000)-32 and G(1)-U(2000)-8 samples. The observation of *T* groups indicated the presence of organosilane groups in the material. The spectral features for all samples were basically the same, but the populations of various silicon environments (T^2 vs T^3) showed some changes as a function of the [O]/[Li] ratio. The T^2/T^3 ratio

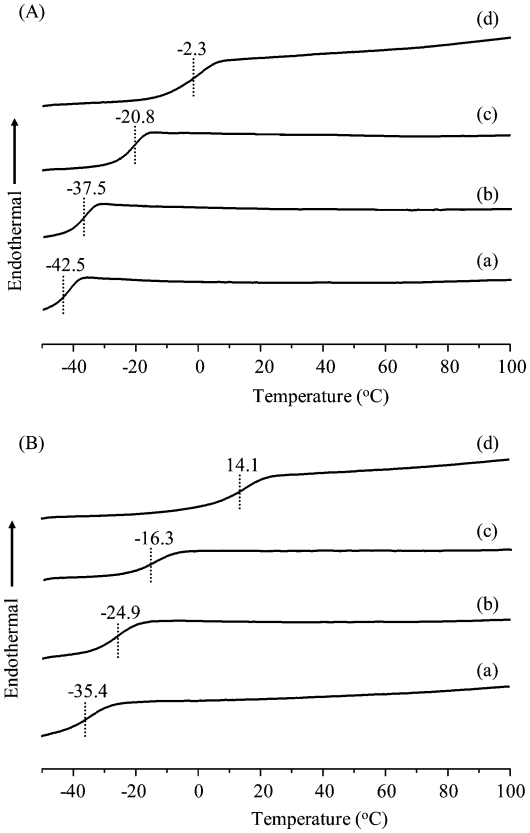

Figure 5. DSC thermograms of (A) G(1)-U(2000)-*Z* and (B) G(1)-U(900)-*Z* hybrid electrolytes with various [O]/[Li] ratios, where Z = (a) 32, (b) 24, (c) 16, and (d) 8. The T_g value was indicated by the dashed line.

Table 2. DSC Results of the Hybrid Electrolytes Studied

	T_g, °C			
Z, [O]/[Li]	G(0)-U(2000)	G(1)-U(2000)	G(1)-U(900)	G(1)-U(600)
32	−32.6	−42.5	−35.4	−7.2
24	−27.6	−37.5	−24.9	−0.1
16	−17.5	−20.8	−16.3	6.1
8	9.4	−2.3	14.1	41.7

progressively changed from 48% for G(1)-U(2000)-32 to 71% for G(1)-U(2000)-8, indicating that the condensation of the silicate network was more complete with lower salt concentrations. The observed difference also reflected that the presence of $LiClO_4$ somehow disturbed the hydrolysis and condensation process for the formation of the silicate networks.

Mobility of Polymer Chains. DSC. The ionic conductivity of SPEs is governed by the content and mobility of the Li ions within the polymer matrix. The mobility is influenced at least by two factors: one is from the mobility of the polymer and the other is the interaction of Li cations with anions and polymer chains. Mobility within the PEO-based electrolytes depends on the segmental motion in the amorphous phase, which is grossly characterized by the glass transition temperature T_g, and the amount of crystalline phase. The thermal behaviors of the hybrid electrolytes doped with various contents of $LiClO_4$ measured by DSC are shown in Figure 5, and the results are also summarized in Table 2. These DSC thermograms showed that all the electrolytes produced, with compositions of [O]/[Li] ratio in the range of 8 to 32, were completely amorphous since no melting transitions were observed. The parent polymer ED2000 has a melting transition at 32.8 °C. After reacting with ICPTES, the T_m value of the ureasil precursor (i.e., G(0)-U(2000)-∞, without GLYMO and salt) shifted to 24.4 °C and was down further to 12.8 °C after the ureasil precursor was further reacted with GLYMO to become G(1)-U(2000)-∞ (see Figure S3, Supporting Information). No melting transition was observed upon doping with lithium salt, and the T_g values were progressively displaced to higher values with increasing salt concentrations for the present hybrid electrolytes. The T_g value is influenced by the intensity of the interactions developed between the polymer segment and the guest salt due to the formation of transient cross-links between the salt and the polyether phase. The presence of such polymer−salt interactions restricts segmental mobility of the host hybrid matrix and thus increases the T_g.

Effect of GLYMO Content on T_g. The effect induced by introduction of GLYMO into the hybrid electrolytes is more evident by comparing the T_g values. In comparison to G(0)-U(2000)-*Z* (Table 2), the G(1)-U(2000)-*Z* samples generally exhibited a lower T_g at a given [O]/[Li] ratio. Since GLYMO also contains some EO segments, the silica domain formed by the co-condensation of ICPTES and GLYMO may solvate some lithium cations, resulting in a decrease in the actual lithium concentration in the polymer host as compared to that without GLYMO. With more GLYMO added in the hybrid electrolytes, however, the G(2)-U(2000)-*Z* samples exhibited similar T_g values as compared to G(1)-U(2000)-*Z*. For example, the T_g values are −42.5 °C for G(1)-U(2000)-32 and −41.0 °C for G(2)-U(2000)-32, and −2.3 °C for G(1)-U(2000)-8 and 1.0 °C for G(2)-U(2000)-8, respectively. This observation implies that the salt solvation ability due to the silica domain is relatively limited, and thus an optimal GLYMO content, GLYMO/ICPTES = 1/2 in the present case, is an important factor for controlling the mobility of the polymer host.

Effects of Polymer Chain Length on T_g. As seen in Table 2, the increase of the PEG fraction of the polymer chains decreased the T_g value for all the lithium concentrations investigated. This indicated that the PEG fraction of the polymers has an effect on the dynamics of the polymer which is substantial enough to influence this bulk property. Since the polymer chains are bonded to the silicate network by covalent bonds via an urea linkage, it is reasonable that the entire chain is closer to the silica node and the segmental motions are thus more hindered for the case of shorter PEG chains, while only a small fraction of the chains is located near the silica interface and the majority of chain segments have high mobility for the case of longer PEG chains. These T_g trends are also corroborated by the ionic conductivity measurements shown below. This feature is similar to the previously reported PEG/silica nanocomposites of type II.[19,24]

^{13}C CPMAS NMR with Variable Contact Time. While DSC measurements help assess the global dynamics of the material, solid-state ^{13}C CPMAS NMR experiments performed with various contact times and 2D ^{1}H−^{13}C WISE NMR are useful to gain more insights into the influence of Li^+ ions on the local dynamics of the polymer chains from the microscopic view. Owing to the complex environments in the region of 72−75 ppm, we focused on the ^{1}H−^{13}C CP signal intensity for the major ether carbon at 71 ppm as a function of contact time and salt doping levels (Figure S4, Supporting Information). The T_{CH} and $T_{1\rho}$(H) measurements were obtained by fitting the CP signal intensities with the following formula:[60]

$$M(t) = M_0 \exp(-t/T_{1\rho}(\mathrm{H}))(1 - \exp(-t/T_{CH})) \qquad (2)$$

where $M(t)$ is the peak intensity as a function of contact time t, M_0 is the normalization constant, $T_{1\rho}$(H) is the proton spin−lattice relaxation in the rotating frame, and T_{CH} is the cross-

polarization time constant. Since CP is a measure of the efficiency of magnetization transfer by the dipolar coupling from ^{1}H to ^{13}C, it is most efficient for the static ^{1}H−^{13}C dipolar interactions. As a result, the less mobile carbon groups exhibit the faster cross-polarization rate or the shorter T_{CH}. The slower growth in spin magnetization for the peak at 71 ppm for G(1)-U(2000)-32 (T_{CH} = 1.4 ms), in comparison to that of G(1)-U(2000)-8 (T_{CH} = 0.3 ms), is consistent with its higher mobility of polymer chains, as also indicated by its low T_g. This reflects that the rapid motion of the former makes the CP signal transfer from the proton spins less efficient than for the latter. The significant decrease in T_{CH} for the peak at 71 ppm with increasing salt concentration suggests a possible coordination of Li^+ ions with the ether oxygen atoms of the polymer chain, thereby restricting the segmental motion and leading to stronger ^{1}H−^{13}C dipolar couplings. Although NMR and DSC techniques probe the materials on a local scale and on a more global scale, respectively, it appears that the NMR results are also consistent with the T_g trends as revealed by DSC.

2D ^{1}H−^{13}C WISE NMR. 2D WISE NMR has been widely used for determining dynamic heterogeneities in solid polymers.[47] With this technique, the spectroscopic information about the dynamic behavior within the present system can be qualitatively assessed by examining the proton line widths associated with the ether carbons in the polymer host. The line width of the ^{1}H line reflects the nature of the dipolar interaction between the protons and thus can be used to monitor the mobility of the polymer chains. For the selected carbon signal at 71 ppm, the G(1)-U(2000)-8 sample exhibited a larger line width (2.55 kHz) in the ^{1}H dimension than the G(1)-U(2000)-32 sample (1.95 kHz) (see Figure S5, Supporting Information). This reflected some microscopically dynamic changes of the polymer chains as the salt content was increased. In comparison to most crystalline or semicrystalline polymers, which always exhibited proton line width larger than 50 kHz, the much narrower proton line width from the 2D WISE NMR revealed considerable chain mobility for the present hybrid electrolytes. Upon addition of more GLYMO, the G(2)-U(2000)-*Z* (*Z* = 32 and 8) samples gave similar line widths in the ^{1}H dimension as to the G(1)-U(2000)-*Z* samples with the same [O]/[Li] ratio. This observation revealed that the mobility of the polymer chains did not have a significant change as more GLYMO was incorporated to form a more rigid organic−inorganic network. The 2D WISE NMR results gained a microscopic insight into the mobility change of the polymer chains as functions of salt concentrations and silica contents, which are also corroborated by the T_g trends as revealed by DSC.

Ionic Conductivity. Figure 6 shows the effects of $LiClO_4$ content and temperature on the ionic conductivity (σ) of the G(1)-U(2000)-*Z* and G(1)-U(900)-*Z* hybrid electrolytes. All the electrolytes showed a VTF (Vogel−Tamman−Fulcher)-like enhancement of the conductivity when the temperature was increased, similar to what was observed for conventional SPEs. The nonlinearity of temperature dependence of ionic conductivity indicates that the ion transport in the present hybrid electrolytes is mainly dependent on the polymer segmental motion. The G(1)-U(2000)-32 electrolyte, with a [O]/[Li] ratio of 32, exhibited the highest ionic conductivity with a value of 1.37×10^{-5} S/cm at 30 °C. Further increase in the salt contents results in a remarkable decrease in the total ionic conductivity, especially for the hybrid electrolyte with the largest amount of lithium salt (i.e., [O]/[Li] = 8). Other hybrid electrolytes with less salt concentrations were also prepared and characterized but with lower conductivity values. The conductivity values

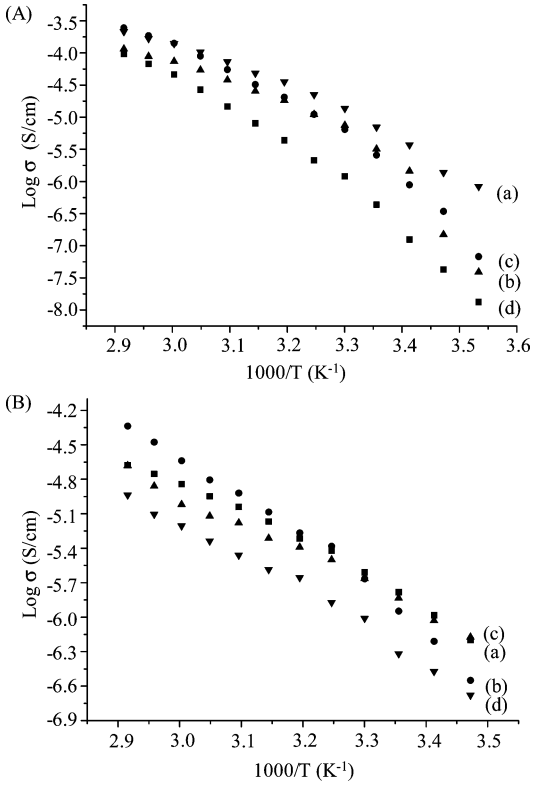

Figure 6. Temperature dependence of ionic conductivity of (A) G(1)-U(2000)-*Z* and (B) G(1)-U(900)-*Z* hybrid electrolytes with various [O]/[Li] ratios, where *Z* = (a) 32, (b) 24, (c) 16, and (d) 8.

Table 3. Conductivity, Li^+ Diffusion Coefficients (Both at 60 °C), and Activation Energies (E_a) Obtained from ^{7}Li Line Width Measurements of the G(1)-U(2000)-*Z* Hybrid Electrolytes

	G(1)-U(2000)		
Z, [O]/[Li]	σ (S/cm)	D_{Li} (cm^2/s)	E_a (kJ/mol)
32	1.39×10^{-4}	7.47×10^{-8}	16.9
24	7.40×10^{-5}	3.08×10^{-8}	22.0
16	1.42×10^{-4}	2.19×10^{-8}	30.7
8	4.64×10^{-5}	1.52×10^{-8}	31.9

obtained for the hybrid electrolyte films as a function of salt concentration are summarized in Tables 1 and 3. It is generally accepted that ionic conductivity in polymer electrolytes is mainly attributed to the presence of the amorphous phase above their glass transition temperatures, which assists the ion mobility. All the present hybrid electrolytes with various Li concentration are in a completely amorphous state. Therefore, this factor can be ruled out for their difference in the ionic conductivity values.

Several factors, such as mobility of polymer chains, cation and anion types, and salt concentration, are important to determine the ionic conductivity in polymer electrolytes. The ionic conductivity of a polymer electrolyte depends on the actual concentration of the conducting species and their mobility and may be given as

$$\sigma(T) = \sum_i n_i q_i \mu_i \tag{3}$$

where n_i is the number of charge carriers, q_i is the charge on each charge carrier, and μ_i is the mobility of charge carriers. According to eq 3, the ionic conductivity depends on the amount of charge carriers in the system and the mobility of the various species. The dissociation of the guest salt into mobile ions is clearly important. Since the polymer environment is a medium of low dielectric constant, the dissociation of the guest salt

depends on the salt concentration and increases as the concentration is reduced. Although the number of charged mobile species is less at higher values of [O]/[Li] ratios, the dissociation of the salt to form charged species is greater, as revealed by IR, at least partially compensating for the effect of lower salt concentration. As the ion transport mechanism in solvent-free polymer electrolytes is dependent on the local motion of polymer segments, which is governed by the T_g, components which increase free volume may be expected to have a beneficial influence on conductivity. At low salt doping levels, the decrease in the free volume is not significant as evident from the lower T_g values (Table 1). Consequently, the conductivity is predominately governed by the mobility of charge carriers, and thus a better ionic conductivity for the hybrid electrolyte with a [O]/[Li] ratio of 32 is obtained, which can be further supported by the diffusion coefficient measurements of the lithium cations. At high salt concentration, or low values of [O]/[Li] ratios, on the other hand, the decrease in segmental mobility arising from transition cross-linking and the increase of ionic association leading to the formation of ion pairs or aggregates are verified by DSC and IR, respectively. Both effects result in a reduction in bulk ionic conductivity at high salt concentrations.

An increase of the inorganic component fraction also has influence on the conductivity of the material. For example, the G(2)-U(2000)-32 sample only exhibited a conductivity value of 9.87×10^{-6} S/cm at 30 °C, which is slightly lower than that of G(1)-U(2000)-32 (1.37×10^{-5} S/cm at 30 °C). To some extent, this is expected given that the silicate network must have a certain blocking effect on long-range ion transport, making remaining conduction pathways more tortuous. It should be noted that the G(0)-U(2000)-32 samples without GLYMO incorporation only exhibited conductivity values of around 1.5×10^{-6} S/cm at 30 °C. Clearly, introduction of GLYMO has a beneficial effect on the enhancement of ionic conductivity by about 1 order of magnitude. On the other hand, the G(2)-U(2000)-8 sample exhibited a conductivity value of 2.80×10^{-6} S/cm at 30 °C, which is slightly higher than that of G(1)-U(2000)-8 (1.21×10^{-6} S/cm at 30 °C). Since the silica domain formed by the GLYMO and ICPTES also contains some ether oxygen atoms to solvate the lithium cations, increasing the silica contents accompanied by the increase in the salt concentration makes positive contribution to the total ionic conductivity.

Local Environment of Li Cation. Three possible Li^+ coordinating locations, namely, the ether oxygen atoms of the polymer and GLYMO and the carbonyl oxygen atoms, may be active in the diureasil-based hybrid structure. To identify and explore the local environments of the mobile species in the present hybrids, variable temperature $^7Li-\{^1H\}$ (i.e., proton decoupled) MAS NMR measurements were performed on the G(1)-U(2000)-8 and G(1)-U(2000)-32 samples. As seen in Figure 7, there is only one distinct ^7Li local environment present in both hybrids over the temperature range investigated. Since the ether oxygen atoms in the polymer host are the major sites for coordination with the Li^+ cations, other sites such as carbonyl carbons and the ether oxygen sites of GLYMO are too minor to be detectable. Moreover, the local environments for the lithium cations complexed with the ether oxygen sites of GLYMO and the polyether chains could be very similar so that a single resonance in the $^7Li-\{^1H\}$ MAS NMR spectra was observed.

^{7}Li Line Width Measurements. It is important to study the motion of the mobile Li-ion in polymer electrolytes because the Li-ion moves in a dynamic environment created by the polymer motion in the amorphous phase and their transport is

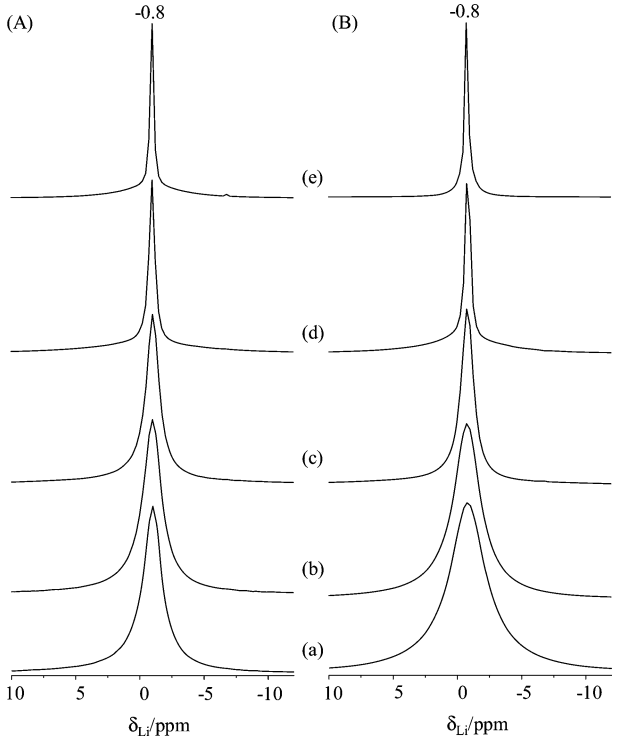

Figure 7. $^7Li-\{^1H\}$ MAS NMR spectra of (A) G(1)-U(2000)-32 and (B) G(1)-U(2000)-8 hybrid electrolytes at (a) −80, (b) −40, (c) −20, (d) 20, and (e) 60 °C, acquired at a spinning speed of 3 kHz.

correlated to the ionic conductivity. The temperature dependence of the static ^7Li line widths is sensitive to the ^7Li motional narrowing process. The spectrum of a spin $^3/_2$ (e.g., ^7Li) system in a powdered crystalline sample is expected to consist of a narrow component due to the $^1/_2 \leftrightarrow -^1/_2$ transition and a Pake doublet due to the $^3/_2 \leftrightarrow {}^1/_2$ and $-^1/_2 \leftrightarrow -^3/_2$ satellite transitions.[60,61] Inspection of the spectra at different temperatures shows that the line shape consists of only a relatively broad line. Since the present hybrid electrolyte is a heterogeneous system, the absence of the satellite quadrupole powder pattern could be due to a wide distribution of possible electric field gradients which results in an almost unobservable Gaussian-broadened line shape for the satellite transitions. For this reason, only the ^7Li central transition was analyzed in this study.

The ^7Li line widths, measured with and without ^1H decoupling, were investigated as a function of temperature from −100 to 80 °C for the G(1)-U(2000)-*Z* samples (Figure 8). The static ^7Li line width evolution as a function of temperature for these materials essentially present similar shapes and can be described by a curve composed of two plateaus separated by a temperature range where a rapid change in line width occurred. At the low-temperature region of −100 to −50 °C, the temperatures much below the T_g of the systems, the line widths were very broad (FWHH = ∼6 kHz) and were slightly narrowed upon increasing temperature, indicating the limited motion of the lithium cations at low temperatures. A significant reduction in the ^7Li line width (from 6.0 to 1.0 kHz) in the low-temperature region (i.e., −100 to −50 °C) was achieved by the use of the proton decoupling techniques. This clearly demonstrated that the line width of ^7Li NMR spectra is predominately governed by $^1H-^7Li$ dipolar interactions (about 85% of all ^7Li spin interactions). Upon an increase in the temperature, the line widths were motionally narrowed, with the onset temperature of narrowing for all these samples is around −50 °C, which is much below their corresponding glass transition temperature (Figure 8). Motional narrowing begins when the rate of the fluctuations (τ_c^{-1}) of

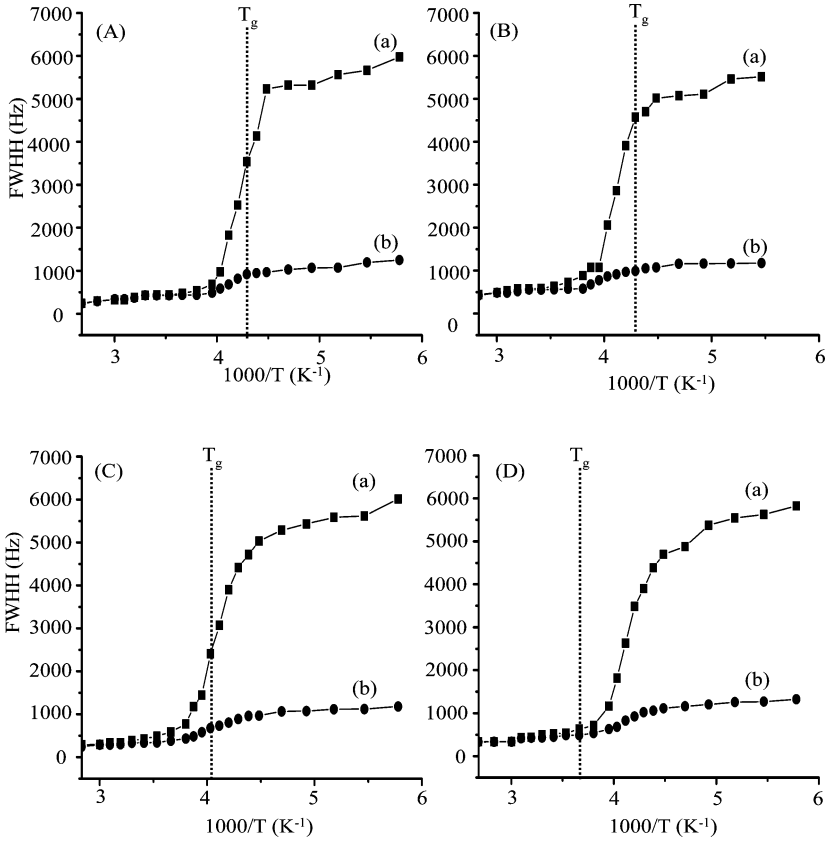

Figure 8. Temperature dependence of ^{7}Li static line widths of G(1)-U(2000)-*Z* hybrid electrolytes with various [O]/[Li] ratios, where *Z* = (A) 32, (B) 24, (C) 16, and (D) 8, measured (a) without and (b) with proton decoupling. The dashed lines represent the T_g values obtained from DSC.

either the local dipolar fields or the electric field gradients (EFG) is comparable to their respective rigid lattice line widths (Δ_{RL}) or when $1/\tau_c \sim \Delta_{RL}$, where τ_c is the motional correlation time.[61] The fluctuations of the local dipolar fields may come from the contribution of the motion of the polymer chains. If this is the case, the onset temperature of ^{7}Li line width narrowing without proton decoupling should be lower than the case with proton decoupling, since the ^{1}H−^{7}Li dipolar coupling was removed in the latter case. As evidenced in Figure 8, however, the onset temperature of ^{7}Li line width narrowing is nearly the same for both experimental conditions. From the microscopic view of NMR, therefore, it can be concluded that the reduction in the line widths of the lithium ion at temperatures below the DSC T_g is mainly due to the averaging of the quadrupolar effects with increasing temperature.

The activation energy, E_a, is an important dynamical parameter that can be indirectly obtained from the NMR data. The NMR motional narrowing of the ^{7}Li line width takes place when the rate of fluctuations of the local magnetic fields or electric field gradients, which are generally described by a correlation time, τ_c, is of the order of the rigid lattice line width, Δ_{RL}

$$1/\tau_c \approx \Delta_{RL} \tag{4}$$

An estimation of the activation energy for the narrowing process, E_a, may be obtained by the relationship[61]

$$\tau_c = \frac{\alpha}{\Delta_{HT}} \tan\left[\frac{\pi}{2}\left(\frac{\Delta_{HT}}{\Delta_{RL}}\right)^2\right] \tag{5}$$

where Δ_{HT} and Δ_{RL} are the FWHHs at a given temperature and in the rigid lattice, respectively, and α is a constant of the order of unity. For all of the samples, the onset temperature of the rigid lattice line width (approximately 6 kHz) occurs at about −50 °C. Assuming that τ_c is thermally activated

$$\tau_c = \tau_0 \exp(E_a/kT) \tag{6}$$

The activation energies, E_a, obtained from ^{7}Li line width measurements by fitting eqs 5 and 6 are listed in Table 3. The activation energies were obtained from the ^{7}Li line width measurements performed without proton decoupling around the transition. As seen in Table 3, the activation energies progressively increased with increasing salt concentrations as expected.

^{7}Li Diffusion and Ionic Conductivity. Whereas the conductivity is a macroscopic quantity, PGSE NMR technique is a more direct NMR method for measuring the ion mobility at the micrometer scale. The most important advantage of the PGSE method over NMR relaxation-based techniques is the direct measurement of diffusion constants (*D*) of the charged carriers without any assumptions. The disadvantage is, however, that the measured values are the population-weighted averages of the various ^{7}Li species, since the self-diffusion coefficients measured by the PGSE NMR method include all the species (i.e., isolated and ion-paired). The representative diffusion curves of G(1)-U(2000)-*Z* as a function of temperature and the ^{7}Li diffusion coefficients measured for the temperature range of 40−100 °C are shown in Figure 9. As seen in Figure 9B, the increase in the ^{7}Li diffusion coefficient was more pronounced at elevated temperatures. Among the samples studied, the G(1)-U(2000)-32 sample with a low salt concentration exhibited the highest ^{7}Li diffusion coefficients over the temperature investigated. Conductivity and ionic diffusion are commonly related by the modified Nernst−Einstein equation:

$$\sigma_{calcd} = Ne^2(D_{Li} + D_{anion})\beta/kT \tag{7}$$

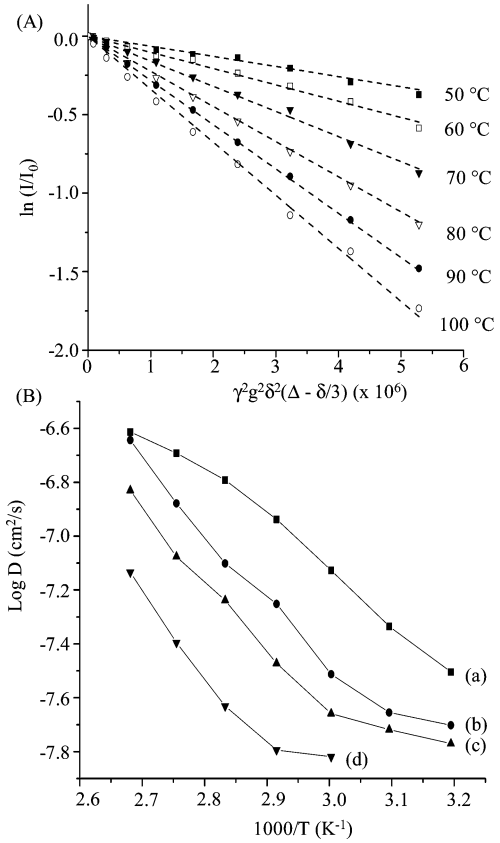

Figure 9. (A) Representative diffusion curves of G(1)-U(2000)-32 as a function of temperature. (B) ^{7}Li diffusion constants of G(1)-U(2000)-*Z* hybrid electrolytes, where $Z =$ (a) 32, (b) 24, (c) 16, and (d) 8, as a function of temperature.

where σ_{calcd} is the calculated ionic conductivity, N is the number of ions per unit volume, e is the charge of the ions, β is the degree of ion dissociation, and D_{Li} and D_{anion} are the diffusion coefficients of the cation and anion, respectively. In this investigation, the diffusion coefficient of the anion (ClO_4^-) is not known due to the difficulty of observing chlorine spins. Nevertheless, some literature demonstrated that the anionic mobility is the same order of magnitude (or greater) than the cationic one from ^{7}Li and ^{19}F PGSE NMR experiments in polymer electrolytes.[62−65] As seen in Table 3, the G(1)-U(2000)-32 sample has the highest ^{7}Li diffusion coefficients, reflecting its high conductivity even with the lowest salt concentration. Therefore, the mobility of the lithium cations is one of the decisive factors for the high conductivity of the present hybrid electrolytes, as revealed by the Li^+ diffusion measurements. Since the ^{7}Li diffusion coefficient is a mean value for all Li nuclei containing entities no matter what their charge, the decrease in the lithium diffusion coefficient with increasing salt concentration could be due to at least two factors: one is the increased amounts of ion pairs and the other is the decrease in segmental mobility arising from the transition cross-linking between the lithium cation and the polymer chain, as demonstrated by IR and DSC, respectively. Both factors may severely inhibit the ion transport process, especially for G(1)-U(2000)-8 with a higher salt concentration. According to eq 3, the bulk ionic conductivity is not only determined by the mobility of the charged carriers but also depends on their numbers. Although the lithium diffusion coefficient of G(1)-U(2000)-16 is lower than that of G(1)-U(2000)-32, the conductivity value obtained at 60 °C for the former is larger. Clearly, the effective numbers of the charged carriers make an important contribution to the conductivity observed for G(1)-U(2000)-16.

Conclusions

The effects of lithium salt concentrations and silica contents on conductivity, polymer segmental motions, and ion structure and dynamics have been investigated in organic−inorganic hybrid electrolytes based on ureasils complexed with $LiClO_4$ via the co-condensation of GLYMO and ICPTES. The multicomponent nature of this system allows these hybrid electrolytes to be fine-tuned by systematically varying the length of backbone PEG chain, the extent of GLYMO cross-linking, and the salt concentration. The highest ionic conductivity value obtained is 1 order of magnitude higher than that of previously characterized electrolytes based on ureasils without incorporation of GLYMO. Multinuclear NMR techniques are useful to provide a microscopic view for probing the specific interaction between the polymer chain and Li^+ cation and the behavior of the mobile ionic species. These combined experiments demonstrate that there is a strong correlation between the behavior of the solid electrolyte and the mobile lithium species.

Acknowledgment. The financial support of this work by the National Science Council of Taiwan is gratefully acknowledged.

Supporting Information Available: IR fitting results of G(1)-U(900) and G(1)-U(600) (Figures S1 and S2); DSC thermograms of pure ED2000, G(0)-U(2000)-∞ and G(1)-U(2000)-∞ (Figure S3); and ^{13}C CPMAS and WISE NMR spectra of G(1)-U(2000) (Figures S4 and S5). This material is available free of charge via the Internet at http://pubs.acs.org.

References and Notes

(1) Fenton, B. E.; Parker, J. M.; Wright, P. V. *Polymer* **1973**, *14*, 589.
(2) Armand, M. *Solid State Ionics* **1994**, *69*, 309.
(3) Meyer, W. H. *Adv. Mater.* **1998**, *10*, 439.
(4) Vincent, C. A.; Scrosati, B. *Modern Batteries: An Introduction to Electrochemical Power Sources*; Butterworth-Heinemann: London, U.K., 1997.
(5) Gray, F. M. *Solid Polymer Electrolytes: Fundamentals and Technological Applications*; VCH: New York, 1991.
(6) Berthier, C.; Gorecki, W.; Minier, M.; Armand, M. B.; Chabagno, J. M.; Rigand, P. *Solid State Ionics* **1983**, *11*, 91.
(7) MacGlashan, G. S.; Andreev, Y. G.; Bruce, P. G. *Nature* **1999**, *398*, 792.
(8) Chung, S. H.; Wang, Y.; Greenbaum, S. G.; Golodnitsky, D.; Peled, E. *Electrochem. Solid-State Lett.* **1999**, *2*, 553.
(9) Golodnitsky, D.; Livshits, E.; Rosenberg, Y.; Lapides, I.; Peled, E. *Solid State Ionics* **2002**, *147*, 265.
(10) Golodnitsky, D.; Livshits, E.; Kovarsky, R.; Peled, E. *Electrochem. Solid-State Lett.* **2004**, *7*, A412.
(11) Hall, P. G.; Davies, G. R.; Melntyre, J. E.; Ward, I. M.; Bannister, D. J.; Le Brocq, K. M. F. *Polymer Commun.* **1986**, *27*, 98.
(12) Nicholas, C. V.; Wilson, D. J.; Booth, C.; Giles, J. R. M. *Br. Polym. J.* **1988**, *20*, 289.
(13) Chen-Yang, Y. W.; Hwang, J. J.; Hung, A. Y. *Macromolecules* **2000**, *33*, 1237.
(14) Allcock, H. R.; Kuharcik, S. E.; Reed, C. S.; Napierala, M. E. *Macromolecules* **1996**, *29*, 3384.
(15) Michot, T.; Mishimoto, A.; Watanabe, M. *Electrochim. Acta* **2000**, *45*, 1347.
(16) Chia, F.; Zheng, Y.; Liu, J.; Reeves, N.; Ungar, G.; Wright, P. V. *Electrochim. Acta* **2003**, *48*, 1939.
(17) Croce, F.; Appetechi, G. B.; Persi, L.; Scrosati, B. *Nature* **1998**, *394*, 456.
(18) Adebahr, J.; Best, A. S.; Byrne, N.; Jacobsson, P.; MacFarlane, D. R.; Forsyth, M. *Phys. Chem. Chem. Phys.* **2003**, *5*, 720.
(19) (a) Mello, N. C.; Bonagamba, T. J.; Panepucci, H.; Dahmouche, K.; Judeinstein, P.; Aegerter, M. A. *Macromolecules* **2000**, *33*, 1280. (b) Dahmouche, K.; Santilli, C. V.; Pulcinelli, S. H.; Craievich, A. F. *J. Phys. Chem. B* **1999**, *103*, 4937.
(20) Ravaine, D.; Seminel, A.; Charbouillot, Y.; Vincens, M. *J. Non-Cryst. Solids* **1986**, *82*, 210.

(21) Popall, M.; Durand, H. *Electrochim. Acta* **1992**, *37*, 1593.
(22) Judeinstein, P.; Livage, J.; Zarudianski, A.; Rose, R. *Solid State Ionics* **1998**, *1722*, 28−30.
(23) (a) Dahmouche, K.; Atik, M.; Mello, N. C.; Bonagamba, T. J.; Panepucci, H.; Aegerter, M.; Judeinstein, P. *J. Sol-Gel Sci. Technol.* **1997**, *8*, 711. (b) Dahmouche, K.; Santilli, C. V.; Da Silva, M.; Ribeiro, C. A.; Pulcinelli, S. H.; Craievich, A. F. *J. Non-Cryst. Solids* **1999**, *247*, 108.
(24) de Souza, P. H.; Bianchi, R. F.; Dahmouche, K.; Judeinstein, P.; Faria, R. M.; Bonagamba, T. J. *Chem. Mater.* **2001**, *13*, 3685.
(25) de Zea Bermudez, V.; Alcacer, L.; Acosta, J. L.; Morales, E. *Solid State Ionics* **1999**, *116*, 197.
(26) Bronstein, L. M.; Joo, C.; Karlinsey, R.; Ryder, A.; Zwanziger, J. W. *Chem. Mater.* **2001**, *13*, 3678.
(27) Dag, Ö.; Verma, A.; Ozin, G. A.; Kresge, C. T. *J. Mater. Chem.* **1999**, *9*, 1475.
(28) Popall, M.; Andrei, M.; Kappel, J.; Kron, J.; Olma, K.; Olsowski, B. *Electrochim. Acta* **1998**, *43*, 1155.
(29) Simon, P. F. W.; Ulrich, R.; Spiess, H. W.; Wiesner, U. *Chem. Mater.* **2001**, *13*, 3464.
(30) Kao, H.-M.; Chen, C.-L. *Angew. Chem., Int. Ed.* **2004**, *8*, 980.
(31) Bronstein, L. M.; Karlinsey, R. L.; Ritter, K.; Joo, C. G.; Stein, B.; Zwanziger, J. W. *J. Mater. Chem.* **2004**, *14*, 1812.
(32) Jiang, S.; Yu, D.; Ji, X.; An, L.; Jiang, B. *Polymer* **2000**, *41*, 2041.
(33) Di Noto, V.; Zago, V.; Biscazzo, S.; Vittadello, M. *Electrochim. Acta* **2003**, *48*, 541.
(34) Dahmouche, K.; Atik, M.; Mello, N. C.; Bonagamba, T. J.; Panepucci, H.; Aegerter, M. A.; Judeinstein, P. *Mater. Res. Soc. Symp. Proc.* **1996**, *435*, 363.
(35) Dahmouche, K.; Atik, M.; Mello, N. C.; Bonagamba, T. J.; Panepucci, H.; Judeinstein, P.; Aegerter, M. A. *Sol. Energy Mater. Sol. Cells* **1998**, *54*, 1.
(36) Dahmouche, K.; Souza, P. H.; Mello, N. C.; Bonagamba, T. J.; Panepucci, H.; Judeinstein, P.; Pulcinelli, S. H.; Santilli, C. V. *J. Sol-Gel Sci. Technol.* **1998**, *13*, 909.
(37) Judeinstein, P.; Titman, J.; Stamm, M.; Schmidt, H. *Chem. Mater.* **1994**, *6*, 127.
(38) Judeinstein, P.; Sanchez, C. *J. Mater. Chem.* **1996**, *6*, 511.
(39) Sanchez, C.; Ribot, F.; Lebeau, B. *J. Mater. Chem.* **1999**, *9*, 35.
(40) Bermudez, V. Z.; Poinsignon, C.; Armand, M. *J. Mater. Chem.* **1997**, *7*, 1677.
(41) Judeinstein, P.; Brik, M. E.; Bayle, J. P.; Courtieu, J.; Rault, J. *Mater. Res. Soc. Symp. Proc.* **1994**, *346*, 937.
(42) Brik, M. E.; Titman, J. J.; Bayle, J. P.; Judeinstein, P. *J. Polym. Sci., Part B: Polym. Phys.* **1996**, *34*, 2533.
(43) (a) de Zea Bermudez, V.; Carlos, L. D.; Alcacer, L. *Chem. Mater.* **1999**, *11*, 569. (b) Stathatos, E.; Lianos, P.; Orel, B.; Surca Vuk, A.; Jese, R. *Langmuir* **2003**, *19*, 7587.
(44) (a) Carlos, L. D.; de Zea Bermudez, V.; Ferreira, R. A.; Marques, L.; Assuncão, M. *Chem. Mater.* **1999**, *11*, 581. (b) Silva, M. M.; de Zea Bermudez, V.; Carlos, L. D.; Passos de Almeida, A. P.; Smith, M. J. *J. Mater. Chem.* **1999**, *9*, 1735. (c) Silva, M. M.; de Zea Bermudez, V.; Carlos, L. D.; Smith, M. J. *Electrochim. Acta* **2000**, *45*, 1467.
(45) (a) Silva, M. M.; Nunes, S. C.; Barbosa, P. C.; Evans, A.; de Zea Bermudez, V.; Smith, M. J.; Ostrovskii, D. *Electrochim. Acta* **2006**, *52*, 1542. (b) Nunes, S. C.; de Zea Bermudez, V.; Ostrovskii, D.; Carlos, L. D. *J. Mol. Struct.* **2004**, *702*, 39.
(46) (a) Nunes, S. C.; de Zea Bermudez, V.; Ostrovskii, D.; Silva, M. M.; Barros, S.; Smith, M. J.; Sá Ferreira, R. A.; Carlos, L. D.; Rocha, J.; Morales, E. *J. Electrochem. Soc.* **2005**, *152*, A429. (b) Nunes, S. C.; de Zea Bermudez, V.; Silva, M. M.; Barros, S.; Smith, M. J.; Morales, E.; Carlos, L. D.; Rocha, J. *Solid State Ionics* **2005**, *176*, 1591. (c) Silva, M. M.; de Zea Bermudez, V.; Carlos, L. D.; Smith, M. J. *Electrochim. Acta* **2000**, *45*, 1467.
(47) Schmidt-Rohr, K.; Clauss, J.; Spiess, H. W. *Macromolecules* **1992**, *25*, 3272.
(48) Stejskal, E. O.; Tanner, J. E. *J. Chem. Phys.* **1965**, *42*, 288.
(49) Mills, R. *J. Phys. Chem.* **1973**, *77*, 685.
(50) Coleman, M. M.; Lee, K. H.; Skrovanek, D. J.; Painter, P. C. *Macromolecules* **1986**, *19*, 2149.
(51) Miyazawa, T.; Shimanouchi, T.; Mizushima, S.-I. *J. Chem. Phys.* **1956**, *24*, 408.
(52) (a) Lee, H. S.; Wang, Y. K.; Hsu, S. L. *Macromolecules* **1987**, *20*, 2089. (b) Lavrenčič, U.; Grošelj, N.; Orel, B.; Colomban, Ph. *Chem. Mater.* **2000**, *12*, 3745. (c) Mattia, J.; Painter, P. *Macromolecules* **2007**, *40*, 1546.
(53) Carlos, L. D.; de Zea Bermudez, V.; Sá Ferreira, R. A. *J. Non-Cryst. Solids* **1999**, *247*, 203.
(54) Nandi, M.; Conklin, J. A.; Salvati, L.; Sen, A. *Chem. Mater.* **1991**, *3*, 201.
(55) Babonneau, F.; Dire, S.; Bonhomme-Coury, L.; Livage, J. *Inorganic and Organometallic Polymers II. Sol-Gel Synthesis of Heterometallic OxoPolymers*; ACS Symposium Series 134; American Chemical Society: Washington, DC, 1994; Chapter 12.
(56) Papke, B. L.; Ratner, M. A.; Shriver, D. F. *J. Phys. Chem. Solids* **1981**, *42*, 493.
(57) Eschmann, J.; Strasser, J.; Xu, M.; Okamoto, Y.; Eyring, E.; Petrucci, S. *J. Phys. Chem.* **1990**, *94*, 3908.
(58) Kioul, A.; Mascia, L. *J. Non-Cryst. Solids* **1994**, *175*, 169.
(59) Templin, M.; Wiesner, U.; Spiess, H. W. *Adv. Mater.* **1997**, *9*, 814.
(60) Mehring, M. *Principles of High-Resolution NMR in Solids*, 2nd ed.; Springer-Verlag: New York, 1983.
(61) Chung, S. H.; Jeffrey, K. R.; Stevens, J. R. *J. Chem. Phys.* **1991**, *94*, 1803.
(62) Johansson, A.; Gogoll, A.; Tegenfeldt, J. *Polymer* **1996**, *37*, 1387.
(63) Gorecki, W.; Jeannin, M.; Belorizky, E.; Roux, C.; Armand, M. *J. Phys.: Condens. Matter* **1995**, *7*, 6823.
(64) (a) Hayamizu, K.; Aihara, Y.; Price, W. S. *J. Chem. Phys.* **2000**, *113*, 4785. (b) Hayamizu, K.; Aihara, Y.; Price, W. S. *Electrochim. Acta* **2001**, *46*, 1475.
(65) Gorecki, W.; Roux, C.; Clémancey, M.; Armand, M.; Belorizky, E. *ChemPhysChem* **2002**, *7*, 620.

MA071541C